JACS
JOURNAL OF THE AMERICAN CHEMICAL SOCIETY
pubs.acs.org/JACS
Article

Charge Transport in Sequence-Defined Conjugated Oligomers

Hao Yu, Songsong Li, Kenneth E. Schwieter, Yun Liu, Boran Sun, Jeffrey S. Moore, and Charles M. Schroeder*

Cite This: J. Am. Chem. Soc. 2020, 142, 4852−4861
Read Online
ACCESS | Metrics & More | Article Recommendations | Supporting Information

ABSTRACT: A major challenge in synthetic polymers lies in understanding how primary monomer sequence affects materials properties. In this work, we show that charge transport in single molecule junctions of conjugated oligomers critically depends on the primary sequence of monomers. A series of sequence-defined oligomers ranging from two to seven units was synthesized by an iterative approach based on the van Leusen reaction, providing conjugated oligomers with backbones consisting of para-linked phenylenes connected to oxazole, imidazole, or nitro-substituted pyrrole. The charge transport properties of these materials were characterized using a scanning tunneling microscope-break junction (STM-BJ) technique, thereby enabling direct measurement of molecular conductance for sequence-defined dimers, trimers, pentamers, and a heptamer. Our results show that oligomers with specific monomer sequences exhibit unexpected and distinct charge transport pathways that enhance molecular conductance more than 10-fold. A systematic analysis using monomer substitution patterns established that sequence-defined pentamers containing imidazole or pyrrole groups in specific locations provide molecular attachment points on the backbone to the gold electrodes, thereby giving rise to multiple conductance pathways. These findings reveal the subtle but important role of molecular structure including steric hindrance and directionality of heterocycles in determining charge transport in these molecular junctions. This work brings new understanding for designing molecular electronic components.

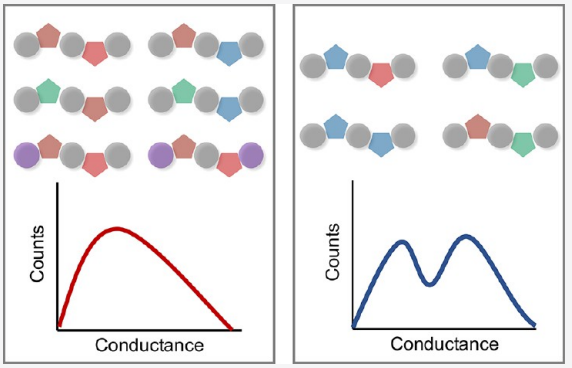

INTRODUCTION

Sequence-defined oligomers (SDOs) and sequence-defined polymers (SDPs) are chain molecules with a precise order of monomer units; each molecule has a monomeric sequence that is identical to every other molecule.[1,2] Sequence definition in nucleic acids and proteins is essential to the molecular blueprint of cellular functions. In synthetic materials, SDOs and SDPs offer a new dimension to manipulate self-assembly,[3,4] catalysis,[5] nanoelectronics,[6] molecular recognition,[7] molecular encoding of information,[8] and phase behavior in polyelectrolytes.[9] Despite many recent advances, relating primary monomer sequence to the physical, chemical, and electronic properties of organic materials remains an unsolved problem.[10,11]

The synthetic availability of precision SDOs has hindered progress in realizing structure−function relations.[1] Major challenges lie in the efficient and scalable production of nonbiological oligomers and polymers with discrete chain lengths and sequences. Indeed, the efficient synthesis of nonbiological SDOs and SDPs has been called a "Holy Grail" of polymer science.[12] Various synthetic methods have been pursued, including iterative synthesis,[13,14] template-based synthesis,[15] and controlled step- or chain-growth statistical polymerization.[6,16−19] Recently, advanced synthesis methods and molecular designs including automated synthesis techniques[20,21] and artificial catalytic molecular machines[22] have been introduced into this burgeoning field and continue to open new avenues for the precise synthesis of sequence-defined materials. However, developing synthetic schemes that afford conjugated backbones remains a key challenge. The most useful synthetic methods would be able to draw from a variety of building blocks such as aromatic carbocyclics and heterocyclics. Such methods make possible the establishment of sequence-property correlations beginning from a discrete reference sequence followed by the addition or replacement of monomers at specific locations and subsequently determining the change in properties.

To date, there have been limited studies correlating sequence and properties in a "monomer by monomer" fashion. Nevertheless, pioneering works from Hawker,[23] Li,[24] Lutz,[25] McNeil,[26] Meyer,[27] Noonan,[28] Segalman,[29] and Zuckermann[30] have highlighted sequence-regulation as a promising and powerful method to control the properties of SDOs and SDPs.

Received: January 2, 2020
Published: February 18, 2020

https://dx.doi.org/10.1021/jacs.0c00043
J. Am. Chem. Soc. 2020, 142, 4852−4861

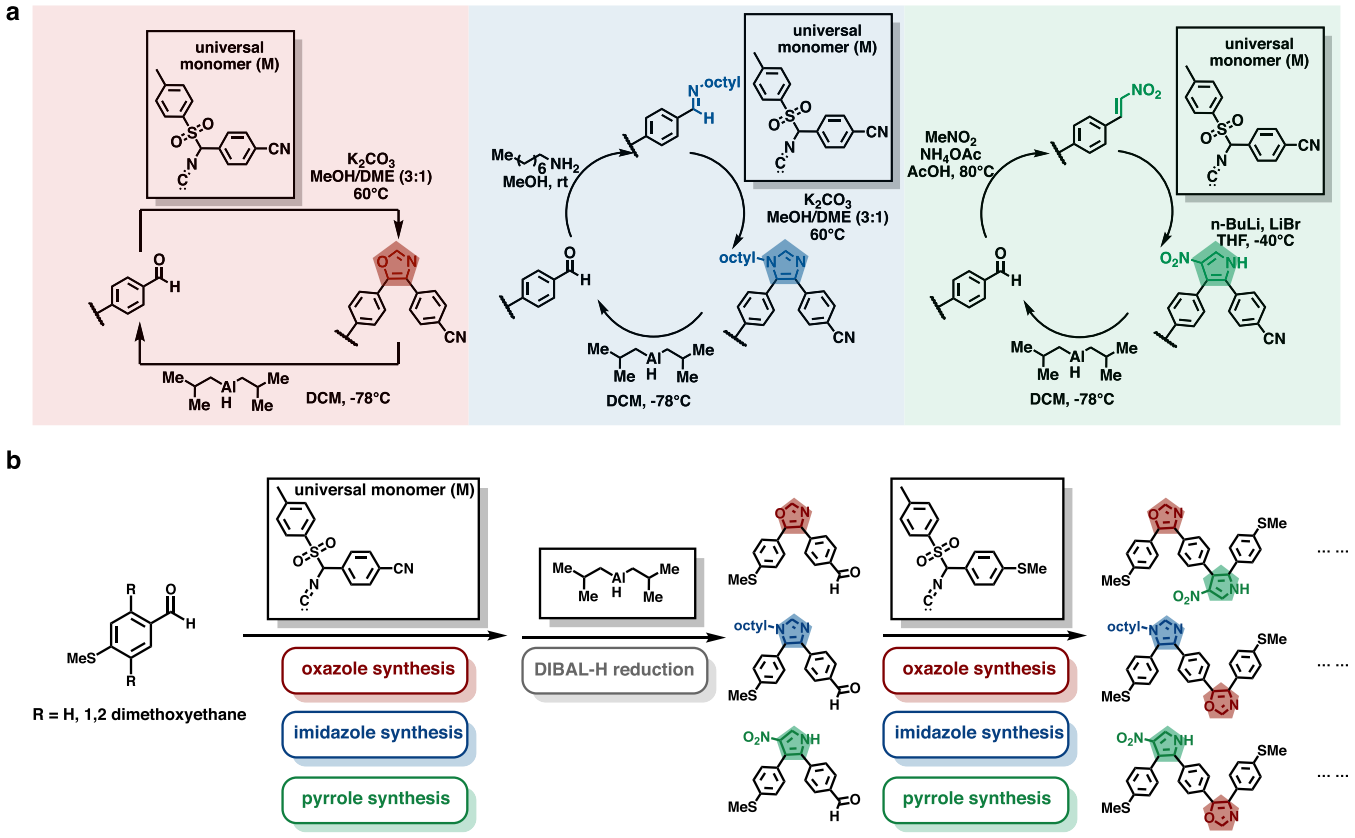

Figure 1. Iterative synthesis of sequence-defined oligomers. (a) Iterative approach consisting of a coupling reaction and a subsequent reduction for the synthesis of alternating para-substituted phenyls linked to oxazole, imidazole, or nitro-substituted pyrrole. (b) Schematic of sequence-controlled synthesis for pentamers. Three different heterocycles (oxazole, imidazole, or nitro-substituted pyrrole) are generated by varying the reaction conditions in each cycle to achieve sequence-defined oligomers. Oligomers are terminated with methyl sulfide to facilitate single molecule conductance measurements.

In SDOs and SDPs, each monomer contributes to the backbone's electronic structure and functional group placement by altering chain conformation and molecular geometry. Intrinsic monomeric contributions to bulk material properties are difficult to disentangle due to the contributions from intermolecular and intramolecular factors. To this end, single molecule techniques offer the ability to directly probe properties at the molecular scale, thereby enabling elucidation of quantitative structure−property relationships (QSPR) for sequence-defined materials.[31,32] Single molecule junctions have been used to study charge transport as a function of molecular length,[33] aromaticity,[34] anchor groups,[35] chemical substituents,[36] gating voltage,[37] molecular conformation,[38] and orbital alignment between molecular bridges and metallic electrodes.[39] The direct measurement of single molecule conductance provides the opportunity to probe the intrinsic relationship between sequence and electronic properties.

In this work, the synthesis of precisely defined conjugated SDOs is described together with single molecule conductance measurements and molecular simulations. We first establish an iterative strategy for synthesizing sequence-defined conjugated oligomers using the van Leusen heterocycle synthesis. This approach was applied to the synthesis of a series of SDOs consisting of alternating *p*-phenylene and heterocyclic units. Unlike traditional iterative synthetic schemes that require chemically distinct monomers, our approach provides sequence definition by altering reaction conditions in each synthetic cycle using a universal monomer. Following synthesis, we directly characterize the molecular conductance and charge transport properties of the SDO library using a scanning tunneling microscope-break junction (STM-BJ) method. Our results show that molecular junctions with specific monomer sequences exhibit multiple distinct charge transport pathways, some of which enhance conductance more than 10-fold. In tandem, we characterize the distinct conductance pathways using a series of structural analogues in concert with molecular modeling. Our results show that the high conductance pathways emerge from gold-molecule linkages through imidazole and nitro-substituted pyrrole located within the oligomer backbone. In this way, geometrical effects including sequence-controlled directionality and steric hindrance of side chains determine intramolecular charge transport in conjugated oligomers. The role of primary monomer sequence and its role on charge transport in molecular junctions is elucidated, which will inform the design of molecular electronic devices.

RESULTS AND DISCUSSION

Synthetic Strategy, Preparation, and Characterization. An iterative approach was developed for synthesizing discrete, conjugated oligomers with wide ranging compositions and sequence variations. Since 1972, tosylmethyl isocyanide (TosMIC) and its aryl-substituted homologues have been widely used as a C−N═C synthon in the synthesis of multiple heterocycles including oxazoles, imidazoles, and pyrroles, which are collectively known as van Leusen multicomponent

https://dx.doi.org/10.1021/jacs.0c00043
J. Am. Chem. Soc. 2020, 142, 4852−4861

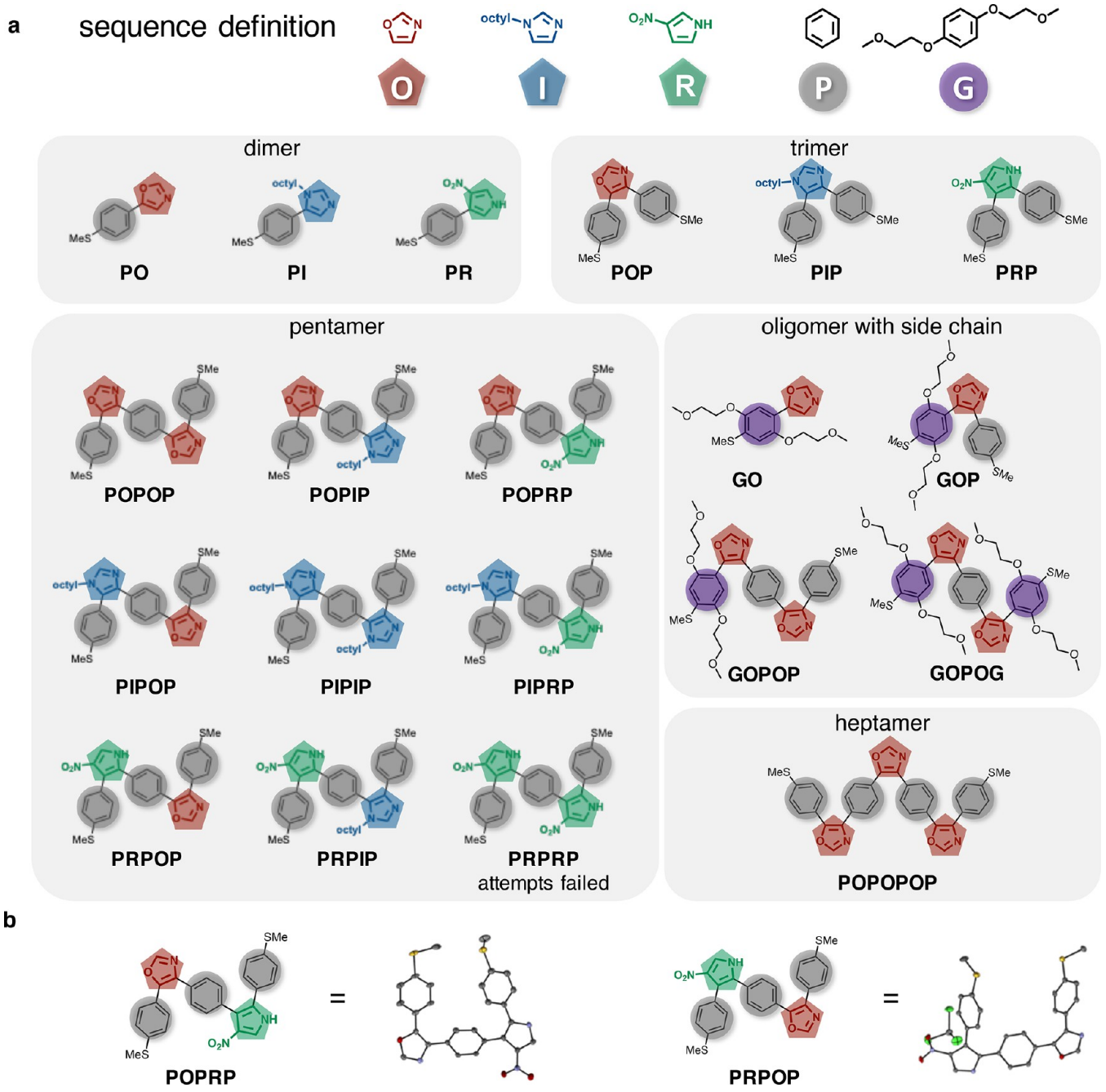

Figure 2. Sequence-defined conjugated oligomers with alternating phenyl heterocycle backbones. (a) Building blocks for sequence definition, O (oxazole), I (imidazole), R (pyrrole), P (phenyl), and G (substituted phenyl). Molecular library of sequence-defined dimers, trimers, pentamers, and heptamer. (b) Crystal structures of **POPRP** and **PRPOP** formed by slow evaporation from a mixed solvent (chloroform/*n*-hexane). Hydrogen atoms are removed for clarity, and a $CHCl_3$ molecule is located within the unit cell of **PRPOP**.

reactions (van Leusen MCRs).[40] Here, we design a monomer (**M**) containing the requisite tosylmethyl isocyanide group for heterocycle synthesis and a latent functionality (nitrile) for subsequent additions by reductive conversion to a terminal aldehyde. The iterative method consists of two steps (Figure 1a): (1) a coupling reaction, which is used to generate a heterocycle (oxazole, imidazole, or nitro-substituted pyrrole) from an aldehyde by proceeding through one of three homologous van Leusen MCRs, and (2) a reduction, which returns an aldehyde from the terminal nitrile using diisobutylaluminum hydride (DIBAL-H), thereby enabling additional coupling reactions in subsequent steps. Oligomers prepared by this approach have an orthro connectivity to the heterocycle, which leads to a twisting between the phenylene and heterocycle in the molecular backbone. Additional diversity was achieved by including chemical substitutions such as 1,2-dimethoxyethane on the phenylene group. Broadly speaking, this strategy allows for preparation of compositionally rich sequences of defined length with a limited set of building blocks.

Using the iterative approach described above, 19 SDOs were prepared ranging in length from dimer to heptamer (Figure 2a). In particular, we synthesized nearly all possible dimeric, trimeric, and pentametric sequences with unsubstituted

https://dx.doi.org/10.1021/jacs.0c00043
J. Am. Chem. Soc. 2020, 142, 4852−4861

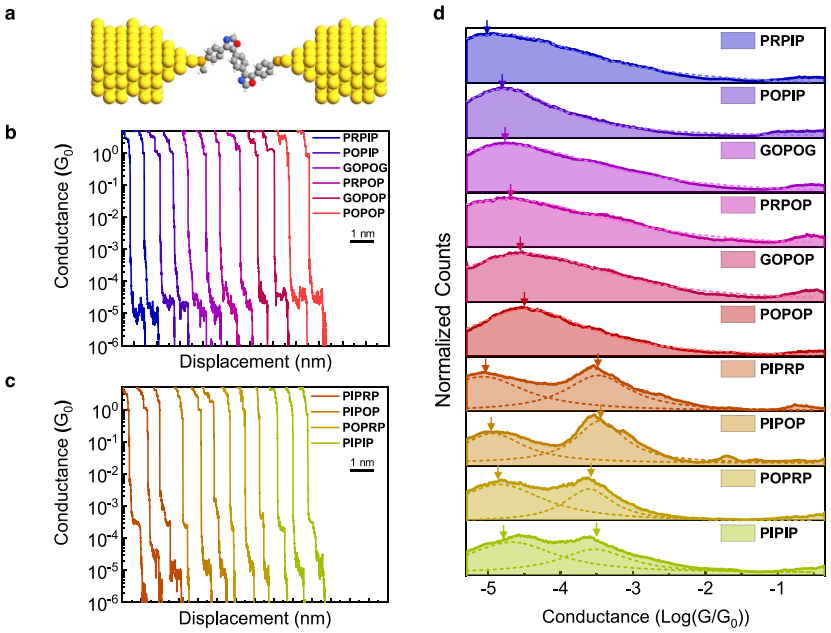

Figure 3. Single molecule conductance of sequence-defined oligomers. (a) Schematic illustration of single molecule break junction. (b) Characteristic single molecule conductance traces of sequence-defined pentamers showing a single conductance peak (applied bias 0.25 V). (c) Characteristic single molecule conductance traces of sequence-defined pentamers exhibiting multiple conductance peaks (applied bias 0.25 V). For these oligomers, two well-spaced conductance peaks are observed (high conductance $10^{-3.5}$ G_0, low conductance 10^{-4}–10^{-5} G_0). (d) Series of 1D conductance histograms for 10 sequence-defined pentamers (applied bias 0.25 V). Some sequences exhibit multiple conductance peaks associated with multiple molecular conductance pathways. Dotted line shows the result of Lorentzian fitting.

phenylene units. Attempts to synthesize the pentamer containing two pyrrole units failed, presumably because of side reactions between the pyrrole-containing precursor and the reagent *n*-butyllithium in the second iterative cycle. Broadly speaking, this methodology is generalizable to synthesize oligomers beyond the heptameric length and the sequence variations described here.

The structure of each SDO was confirmed by ^{1}H and ^{13}C NMR spectroscopy and mass spectrometry (Supporting Information, SI, Sections S1–S3 and Figures S1–S80). Sequence-defined oligomers are referred to using a naming convention based on the substituent building blocks (Figure 2). Pentamers containing the same composition but with different sequences are structurally distinct. For example, **PIPOP** and **POPIP** are constitutional isomers with different heterocycle directionalities that may impact charge transport, as discussed below. A pair of isomeric pentamers, **POPRP** and **PRPOP**, crystallized as slender prisms under ambient conditions. Single-crystal X-ray diffraction analysis reveal that both oligomers have similar twisted U-shaped conformations in the solid state (Figure 2b). Interestingly, primary sequence also plays an important role in solid state structures such that **POPRP** and **PRPOP** have different packing patterns (SI Figures S81–S84). By using different solutions as mixed solvents (chloroform/*n*-hexane or ethyl acetate/*n*-hexane), we also observed two polymorphs of **POPRP** (SI Tables S1 and S2 and Figures S81 and S82) and one solvatomorph of **PRPOP** (SI Tables S3 and S4 and Figures S83 and S84).

Single Molecule Conductance of Sequence-Defined Oligomers. We employed a single molecule measurement—electronic conductance—to directly measure the charge transport properties of each SDO. In particular, molecular conductance is determined using a scanning tunneling microscope-break junction (STM-BJ) technique as previously described (Figure 3a and SI Sections 5 and Figures S85–S105).[41] In all cases, experiments are repeated on at least 10^{3}–10^{4} individual molecules using the STM-BJ technique to enable robust statistical analysis. The SDOs contain dual terminal methyl sulfide (-SMe) groups that serve as anchors for making robust connections to gold electrodes.[33,41−43] Individual molecular conductance traces (Figures 3b,c) are compiled into one-dimensional (1D) histograms without data selection (Figure 3d). In this way, 1D conductance histograms enable determination of the average molecular conductance by fitting the histogrammed data to a Lorentzian function.[44] For the alternating phenylene-heterocycle oligomers in this work, we generally observe an average molecular conductance in the range between ~10^{-3}–10^{-5} G_0 (Tables S5–S7), where G_0 = 77.5 μS is the quantum unit of conductance. The ortho connectivity around heterocycles leads to a twisting between the heterocycle and phenylene, which slightly lowers the molecular conductance compared to fully planar structures, such as oligothiophene.[33]

Molecular conductance in the pentamer series shows a remarkable sequence-dependent behavior. For example, conductance histograms of two compositionally identical pentamers **POPIP** and **PIPOP** are markedly different (Figures S86, S89, and S93), such that **POPIP** shows a predominant single peak at low conductance whereas **PIPOP** exhibits two well-spaced peaks in molecular conductance (Figure 3d). We observed two dominant and well-spaced conductance peaks (high G and low G) in pentamers with sequences—**PIPRP**, **PIPOP**, **POPRP**, and **PIPIP** (Figures 3c,d, and S86). Specifically, the conductance of the high G state ($10^{-3.5}$ G_0) is more than one order of magnitude larger than the corresponding low G state (10^{-4}–10^{-5} G_0) for this set of pentamers. Alternatively, a different set of pentamers (**PRPIP**, **POPRP**, **GOPOG**, **PRPOP**, **GOPOP**, and **POPOP**) exhibits a

https://dx.doi.org/10.1021/jacs.0c00043
J. Am. Chem. Soc. 2020, 142, 4852−4861

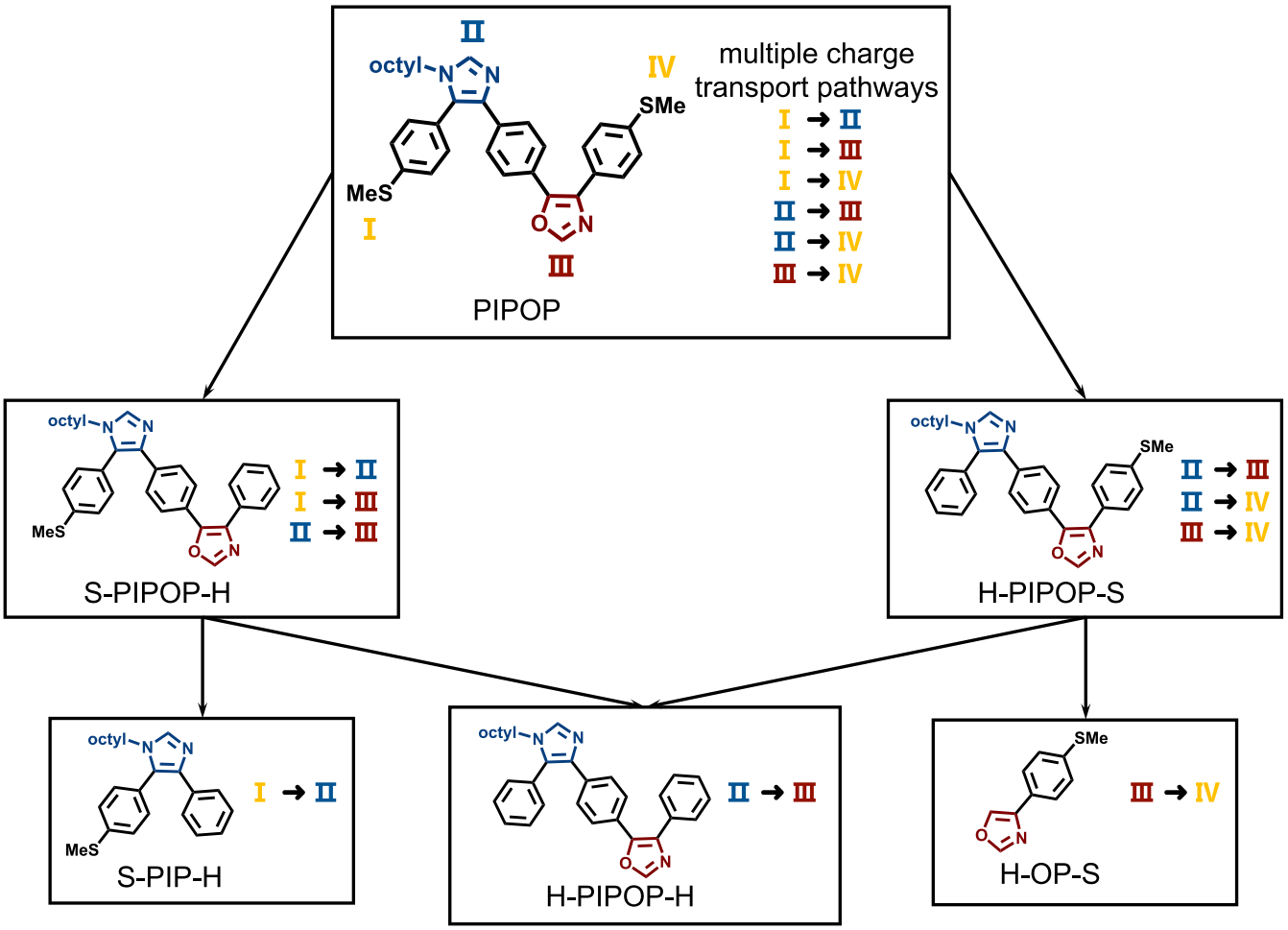

Figure 4. Structural deconstruction to determine conductance pathways. The pentamer **PIPOP** has six possible charge transport pathways corresponding to conductance from the terminal anchors and/or intramolecular heterocycles. Here, we synthesized five control compounds with lower structural complexity providing suitable models to understand the conductance pathway of the pentamer. In this way, the compounds **H-PIPOP-H**, **S-PIP-H**, and **H-OP-S** only contain a single well-defined conductive pathway.

primary conductance peak around 10^{-4}–10^{-5} G_0 and a possible obscured or weak shoulder at a higher molecular conductance around $10^{-3.5}$ G_0. To quantitatively characterize this behavior, we used a Lorentzian fitting method to determine the relative dominance or ratio of the primary conductance peak to possible shoulders or obscured peaks (SI Sections 5.4 and Figures S106–S111). Our results show that the pentamers **PRPIP**, **POPIP**, **GOPOG**, **PRPOP**, **GOPOP**, and **POPOP** are well described by a primary conductance peak, which suggests that charge transport primarily occurs through a single dominant molecular conductance state. Together, these results imply that the charge transport pathway in the pentamer series is dependent on primary sequence. Finally, molecular conductance results for trimers (**POP**, **PIP**, **PRP**, and **GOP**) and a heptamer (**POPOPOP**) with heterocycles located in the backbone generally show 1D conductance histograms with a single statistical conductance value (Figures S85, S86, and S99).

Identifying Sequence-Controlled Conductance Pathways. Compositional variations among the 19 SDOs introduce multiple conductance pathways owing to the possibility that internal heterocycles provide anchor points between the conducting molecule and the gold electrodes. In particular, the nitro group in pyrrole **R** is known to serve as a dative anchor for making robust linkages to gold electrodes.[45,46] Recent work has shown that oxazole **O** serves as an efficient chemical anchor to gold electrodes for single molecule electronics,[47] and the imidazole **I** has a free lone electron pair on the nitrogen atom that can potentially serve as an in-backbone anchoring site to gold electrodes.[48,49]

A systematic structural deconstruction method was used to identify the charge transport pathways of distinct conductance in the pentameric SDOs. We began by focusing on the pentamer **PIPOP** and systematically examined a series of related fragments including **H-OP-S** (dimer), **S-PIP-H** (trimer lacking thiomethyl anchor on one terminus), **S-PIPOP-H** (pentamer lacking thiomethyl anchor on one terminus), **H-PIPOP-S** (pentamer lacking thiomethyl anchor on one terminus), and **H-PIPOP-H** (pentamer lacking thiomethyl anchor on both termini) (Figure 4). These lower structural complexity analogs of **PIPOP** generally consist of subsegments of the pentamer or molecules lacking terminal thiomethyl anchors. In this way, the charge transport pathways in these short molecular analogs are well-defined, which provides a logical and systematic approach to experimentally deconstruct conductance pathways in pentamers of varying sequence.

The molecular conductance of the parent pentamer and its simpler analogs were further analyzed using two-dimensional (2D) histograms of conductance versus displacement. Prior STM-BJ measurements have shown that the maximum

https://dx.doi.org/10.1021/jacs.0c00043
J. Am. Chem. Soc. 2020, 142, 4852–4861

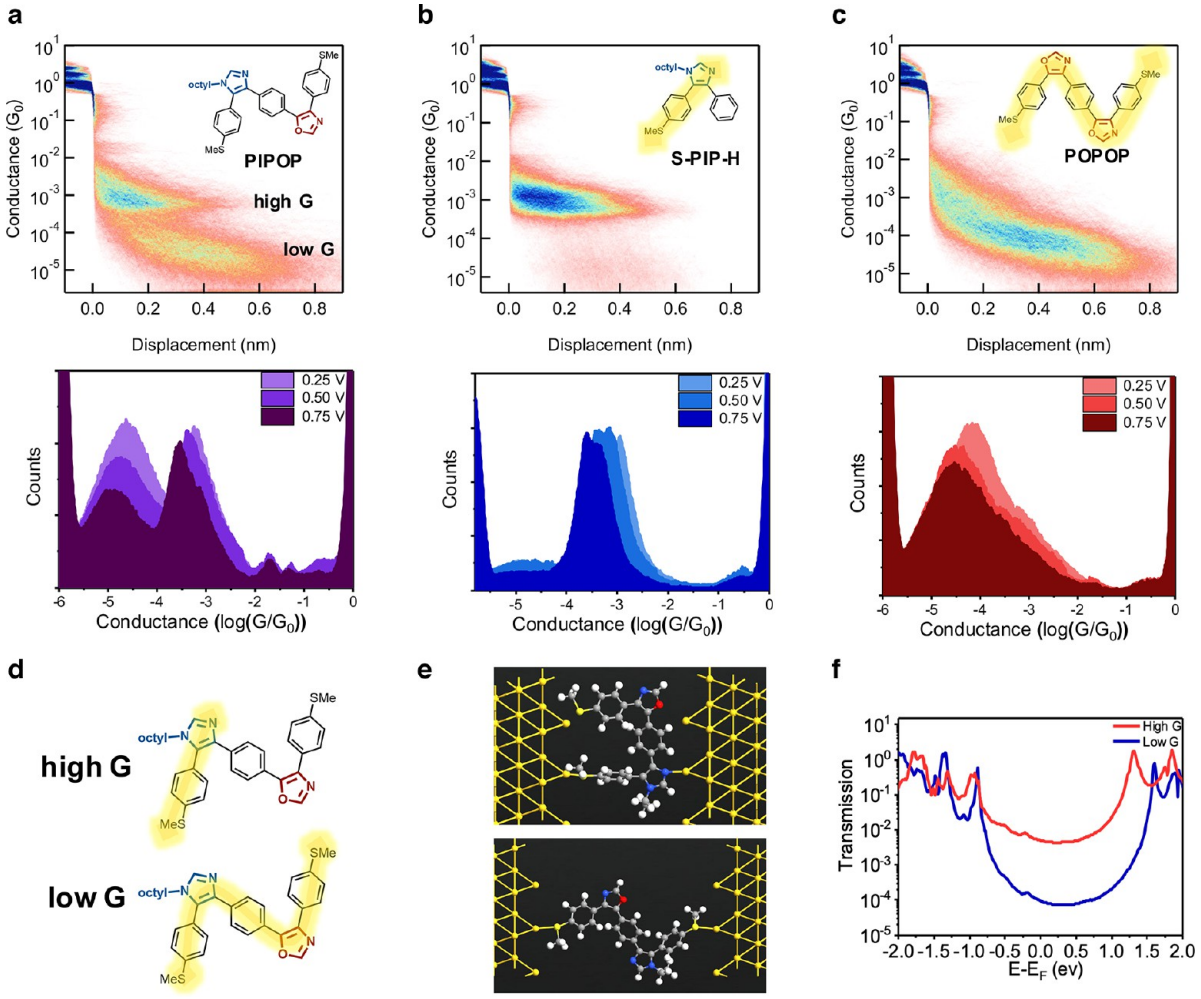

Figure 5. Molecular conductance pathways in sequence-defined pentamers. 2D (top) conductance histograms at 0.75 V applied bias and 1D (bottom) conductance histograms (at 0.25 V, 0.50, and 0.75 V) of (a) **PIPOP**; (b) **S-PIP-H**; and (c), **POPOP**. (d) Mechanism for high conductance (high *G*) and low conductance (low *G*) pathways for **PIPOP**. (e) Molecular conformations for single molecule junctions in NEGF-DFT simulations for determining transmission spectra for two distinct conductance pathways for **PIPOP**. (f) Transmission probabilities of two distinct conductance pathways of **PIPOP** from NEGF-DFT simulations.

displacement between the tip and substrate at which finite conductance is measured is strongly correlated with the contour length of the molecular junction.[50,51] As shown in Figure 5a, the 2D conductance histograms for the pentamer **PIPOP** show that the high *G* conductance state is associated with a small tip-to-substrate displacement of ca. 0.4 nm, whereas the low *G* conductance state occurs with larger molecular extensions of ca. 0.6 nm. This observation suggests that the high *G* state is associated with charge transport through shorter segments of the pentamer compared to the low *G* state.

To understand the high *G* charge transport pathway of the pentamer **PIPOP**, we began by characterizing the molecular conductance of **S-PIP-H** (Figures 5b and S101), which has a defined charge transport pathway through the terminal thiomethyl anchor and the internal imidazole. Our results show that **S-PIP-H** exhibits a molecular conductance that is consistent with the high *G* state of **PIPOP** (Figure 5a) both in displacement and magnitude, across a wide range of applied bias (0.25 V, 0.50, and 0.75 V) (Figures S89 and S101). These results are consistent with conductance in the dimer **PI** (Figure S87c) and likely arise by attaching the backbone to the gold electrode with terminal thiomethyl anchor on one end and the central imidazole on the other. Moreover, the structural analog **S-PIPOP-H** (Figure S100) exhibits a similar high *G* conductance state as **S-PIP-H** (Figure S101), which is again attributed to charge transport through in-backbone imidazole linkages. Interestingly, none of the other simpler analogs of **PIPOP** show a high *G* conductance state observed in the parent pentamer **PIPOP** (Figures S102 and S103). Taken together, these results strongly suggest that the high *G* conductance pathway of **PIPOP** arises from charge transport through the terminal thiomethyl anchor and the internal imidazole.

Next, we analyzed the monothiolated control compounds **S-PIP-H**, **S-PIPOP-H**, and **H-PIPOP-S** to reveal the nature of the low *G* charge transport pathway. We found that these compounds generally exhibit conductance over a maximum displacement of ca. 0.4−0.5 nm (Figures S100−S102), whereas the low *G* state of **PIPOP** exhibits a molecular extension above 0.6 nm (Figure 5a). Moreover, control compounds **S-PIP-H** and **S-PIPOP-H** only exhibit the high *G* state consistent with **PIPOP**. However, the molecular conductance and displacement of the low *G* state of **PIPOP** is consistent with pentamers that show a single conductance pathway such as **POPOP** (Figures 5c and S93−S98).

https://dx.doi.org/10.1021/jacs.0c00043
J. Am. Chem. Soc. 2020, 142, 4852−4861

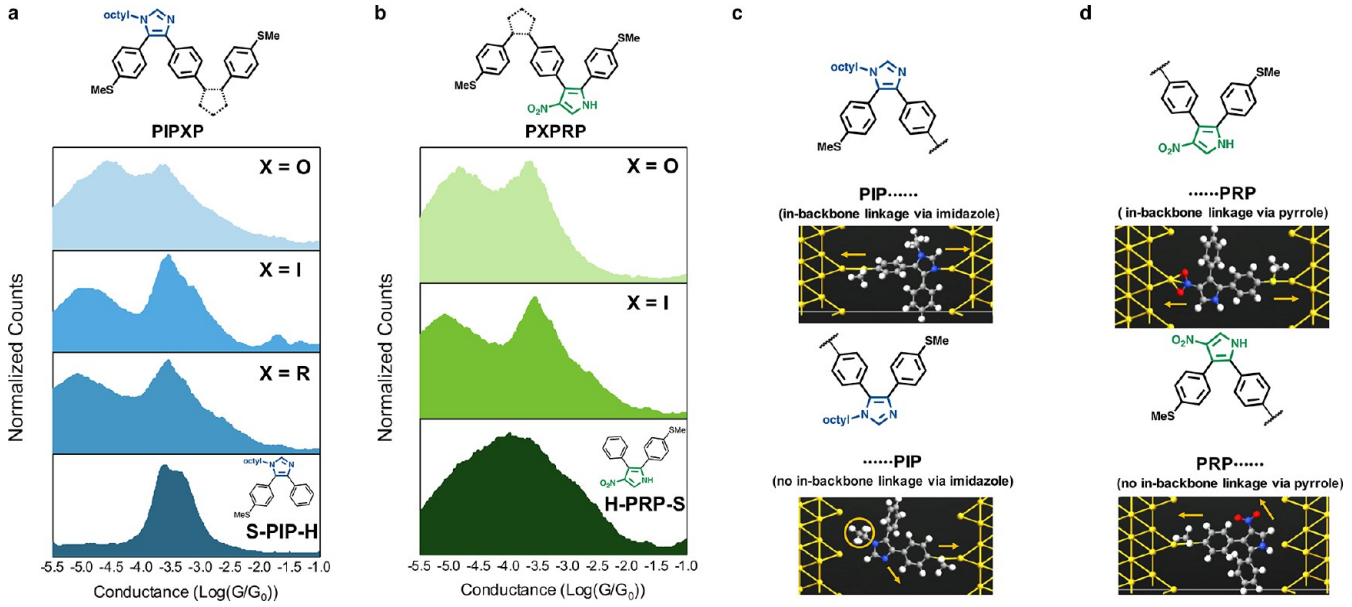

Figure 6. The effect of sequence on charge transport in molecular junctions. (a) Comparison of control compound **S-PIP-H** with pentamers containing the general sequence **PIPXP** (where **X** represents an arbitrary heterocycle such as oxazole, imidazole, or nitro-substituted pyrrole) at 0.25 V. (b) Comparison of control compound **H-PRP-S** with pentamers containing the general sequence **PXPRP** sequence at 0.25 V. (c) Geometrical evaluation of imidazole at different positions from NEGF-DFT simulations. (d) Geometrical evaluation of pyrrole at different positions from NEGF-DFT simulations. The directionality of **PIPXP** and **PXPRP** facilitates in-backbone linkages through imidazole or nitro-substituted pyrrole, thereby leading to a high *G* state. However, in-backbone linkages (high *G*) for **PXPIP** and **PRPXP** are inhibited due to unfavorable geometries and steric hindrance effects.

Together, these results suggest that the low *G* conductance state is associated with a charge transport pathway through the two terminal methyl sulfide anchors. These results are in agreement with prior work by Gonzalez[49] and Lu,[52] where the end-to-end molecular charge transport pathway was generally found to exhibit a lower conductance compared to in-backbone charge transport. Our findings are summarized in a schematic in Figure 5d that shows the observed charge transport pathways for the pentamer **PIPOP**.

Molecular Origin of Sequence-Controlled Conductance Pathways. Molecular modeling using nonequilibrium Green's function-density functional theory (NEGF-DFT) is a useful way to understand charge transport pathways in sequence-defined oligomers. In all cases, molecular geometries are optimized using DFT calculations performed on Spartan'16 Parallel Suite using the B3LYP functional with a 6-31G (d,p) basis set, followed by determination of transmission functions for relaxed molecules via the Atomistix Toolkit package (Figure 5e). NEGF-DFT simulations show that molecular conductance through in-backbone imidazole linkages is >10× larger than conductance through the entire end-to-end molecular contour (Figure 5f). These results are consistent with the experimental results based on simpler control compounds derived from the reference pentamer.

We excluded the possibility that the high *G* conductance state arises from multipodal linkages between the oligomers and the gold tip and substrate. For example, it has been observed that 1,2-disilaacenaphthenes[51] exhibit a relatively high conductance state arising due to multipodal linkages between the molecule and electrode surface. However, in our control experiments, the high *G* conductance state is observed in **S-PIP-H**, which only has two anchors including the central imidazole and terminal methyl sulfide. These results strongly suggest that the multipodal linkage mechanism is likely not observed in the phenylene heterocycle oligomers in this work.

Prior work has also shown that transient molecular conformations leads to a switching of conductance states in oligosilanes[53] and oligogermanes;[54] however, this potential mechanism is not observed in our molecular library. DFT calculations show that the majority of pentamers have two conformations in solution: (1) a Z-shaped conformation, where the molecular backbone has a zigzag geometry, and (2) a U-shaped conformation, where the oligomer backbone has a hairpin shape (Figure S112−S121). In particular, we found that the 1,2-dimethoxyethane side chain has a strong influence on the ratio of the Z-shaped conformation versus U-shaped conformation. For example, the Z/U conformational ratio of **POPOP**, **GOPOP**, and **GOPOG** gradually decreases from 2:1 to 0:1, such that **GOPOG** exclusively adopts the U-shaped geometry. Overall, our results show that these different molecular conformations generally exhibit similar conductance states.

We next considered the high *G* conductance states of the pentamer subset consisting of molecules **PIPOP**, **PIPIP**, **PIPRP**, and **POPRP**. The high *G* conductance states of **PIPOP**, **PIPIP**, and **PIPRP** are consistent with control compound **S-PIP-H** both in displacement and magnitude under different applied biases (0.25 V, 0.50, and 0.75 V) (Figures 6a and S89−S91). This result demonstrates that the high *G* conductance state of pentamers with a **PIPXP** sequence (where **X** represents an arbitrary heterocycle such as oxazole, imidazole, or nitro-substituted pyrrole) all derive from an identical imidazole in-backbone linkage. In order to understand the nature of high *G* conductance of pentamers with a **PXPRP** sequence (**POPRP** and **PIPRP**), we further considered the oligomeric fragment **H-PRP-S** which is a trimeric structure lacking a thiomethyl anchor on one terminus

https://dx.doi.org/10.1021/jacs.0c00043
J. Am. Chem. Soc. 2020, 142, 4852−4861

(Figure 6b). Comparing **POPRP** and **PIPRP** with **H-PRP-S**, we attribute the high *G* conductance state to an in-backbone linkage through the nitro-substituted pyrrole and terminal methyl sulfide (Figures 6b and S90 and S92). The slight difference in conductance magnitudes between **POPRP**, **PIPRP**, and control compound **H-PRP-S** is likely due to differences in conjugation in each molecular structure. The results are consistent across a wide range of bias voltages (0.25 V, 0.50, and 0.75 V) (Figures S104 and S105). Nevertheless, we note that **PIPRP** contains both imidazole and nitro-substituted pyrrole that may form in-backbone linkages, such that conductance in **PIPRP** could arise due to a combination of two different in-backbone linkages.

To more deeply understand the molecular origins of monomer sequence on conductance, we considered the effects of electrode-molecule alignment due to backbone geometry and conformation, monomer orientation, and steric interactions. Interestingly, we observe dual conductance peaks for **PIPOP**, **PIPRP**, and **POPRP**, but only a single conductance peak for their regioisomers **POPIP**, **PRPIP**, and **PRPOP**, despite both sets of molecules having the identical composition in terms of in-backbone anchor groups (**PIPOP** versus **POPIP**, **PIPRP** versus **PRPIP**, and **POPRP** versus **PRPOP**). Imidazole and nitro-substituted pyrrole groups link to gold electrodes by a noncovalent coordination interaction, and the donor−acceptor linkage is expected to be highly orientated as reported prior literature.[43,48] We therefore posit that the alignment between in-backbone anchor sites and adjacent terminal anchoring groups is critically important for forming robust in-backbone linkages. To test this hypothesis, we carried out DFT simulations for geometrical analysis of the metal−molecule junction. Indeed, DFT results show that favorable in-backbone linkages are formed in structures beginning with a **PIP** sequence (e.g., **PIPXX**), which is greatly facilitated by a linear alignment between the imidazole anchor and the terminal methyl sulfide in a two-electrode STM-BJ configuration (Figure 6c). However, for structures ending with a **PIP** sequence (e.g., **XXPIP**), a robust in-backbone linkage is not formed largely because the relative angle between the terminal methyl sulfide and the second anchor site is much smaller than 90°. Moreover, octyl side chains on the substituted imidazole group also introduce strong steric hindrance in molecular junctions, which further inhibit in-backbone linkages.

Similar results are observed in cases where the in-backboned linkage is formed by a nitro-substituted pyrrole. In particular, we observe that robust in-backbone linkages are only formed in structures ending with a **PRP** sequence (e.g., **XXPRP**), wherein alignment between the in-backbone anchor (nitro-substituted pyrrole) and the terminal anchor (methyl sulfide) is nearly linear (Figure 6d). This result is consistent with our experimental observation that only pentamers with these two sequence characteristics (**PIPXX** or **XXPRP** sequence) exhibit two well-spaced conductance peaks (Figures 6a,b). In general, we find that the alignment between the in-backbone anchor and the terminal anchor is critically important in the formation of in-backbone linkages.

We further note that in-backbone oxazole heterocycles generally do not form robust linkages to gold electrodes in our sequence-defined oligomers. Prior work has shown that the electron-donating ability of a lone electron pair is a key dominant factor for determining coupling strength.[48] Due to the strong electronegative character of oxygen, we posit that the nitrogen atom in oxazole heterocycle has a relatively weak electron-donating ability compared to the nitrogen atom in imidazole. Such concepts are also familiar from coordination chemistry; for example, the reported basicity of oxazole (pK_a = 0.8 for the conjugate acid) and imidazole (pK_a = 6.9 for the conjugate acid) are consistent with our conjecture.[55] Overall, our results on sequence-controlled conductive pathways are best explained in the context of geometrical directionality and local steric hindrance. Together, these results may prove generalizable beyond the chemical structures described here and could provide a design framework to understand sequence-effects in molecular electronics.

CONCLUSIONS

In summary, we have demonstrated that the charge transport pathway in conjugated SDOs is precisely controlled by primary sequence, which mainly results from sequence-controlled electrode-molecule alignment. Using an iterative synthetic approach, the position and directionality of three distinct heterocycles (oxazole, imidazole, and nitro-substituted pyrrole) are precisely controlled along π-conjugated backbones for oligomers ranging in size from dimers, trimers, pentamers, and a heptamer. Among 19 SDOs and dozens of control compounds, single molecule conductance measurements show that four pentamers with specific sequences exhibit two distinct conductance pathways consisting of a high conductance state (ca. $10^{-3.5}$ G_0) and a low conductance state (ca. 10^{-4}−10^{-5} G_0). By extensively studying a series of structural analogues coupled with molecular modeling and simulations, we find that the high conductance state arises from charge transport through an in-backbone linkage of imidazole or nitro-substituted pyrrole, whereas the low *G* conductance state arises from charge transport through terminal methyl sulfide anchor groups. The insights provided from NEGF-DFT simulations suggest that a linear metal-molecule alignment geometry and minimal steric hindrance between the metallic electrode and side chain facilitate the in-backbone linkage through heterocycles. Broadly speaking, the synthesis scheme developed in this work will enhance the capabilities of preparing sequence-defined materials with controlled charge transport pathways. In addition, the realization of underlying factors such as molecular geometry and steric interactions that are regulated by primary sequence will enable new strategic molecular design strategies to build materials with sequence-dependent properties.

ASSOCIATED CONTENT

Supporting Information

The Supporting Information is available free of charge at https://pubs.acs.org/doi/10.1021/jacs.0c00043.

Description of chemical synthesis, chemical and physical characterization of oxazole-terminated molecules, experimental details on STM-BJ, simulation methods, supporting text, and supporting figures (PDF)
Crystallographic data (CIF)
Crystallographic data (CIF)
Crystallographic data (CIF)
Crystallographic data (CIF)

AUTHOR INFORMATION

Corresponding Author

Charles M. Schroeder − *Department of Chemical and Biomolecular Engineering, Department of Materials Science and Engineering, Department of Chemistry, and Beckman Institute*

https://dx.doi.org/10.1021/jacs.0c00043
J. Am. Chem. Soc. 2020, 142, 4852−4861

for Advanced Science and Technology, University of Illinois at Urbana—Champaign, Urbana, Illinois 61801, United States; orcid.org/0000-0001-6023-2274; Email: cms@illinois.edu

Authors

Hao Yu − *Department of Chemical and Biomolecular Engineering, University of Illinois at Urbana—Champaign, Urbana, Illinois 61801, United States*

Songsong Li − *Department of Materials Science and Engineering and Beckman Institute for Advanced Science and Technology, University of Illinois at Urbana—Champaign, Urbana, Illinois 61801, United States*

Kenneth E. Schwieter − *Department of Chemistry, University of Illinois at Urbana—Champaign, Urbana, Illinois 61801, United States*

Yun Liu − *Department of Chemistry and Beckman Institute for Advanced Science and Technology, University of Illinois at Urbana—Champaign, Urbana, Illinois 61801, United States;* orcid.org/0000-0001-7077-363X

Boran Sun − *Department of Chemical and Biomolecular Engineering, University of Illinois at Urbana—Champaign, Urbana, Illinois 61801, United States*

Jeffrey S. Moore − *Department of Materials Science and Engineering, Department of Chemistry, and Beckman Institute for Advanced Science and Technology, University of Illinois at Urbana—Champaign, Urbana, Illinois 61801, United States;* orcid.org/0000-0001-5841-6269

Complete contact information is available at: https://pubs.acs.org/10.1021/jacs.0c00043

Author Contributions

H.Y. and S.L. contributed equally to this work.

Notes

The authors declare no competing financial interest.

■ ACKNOWLEDGMENTS

We thank Latha Venkataraman and Yaping Zang for generously providing advice in building the STM-BJ instrument. We also thank Prapti Kafle and Ying Diao for useful discussions and Toby Woods for X-ray diffraction analysis. This work was supported by the U.S. Department of Defense by a MURI (Multi-University Research Initiative) through the Army Research Office (ARO) through Award W911NF-16-1-037 to C.M.S. and J.S.M.

■ REFERENCES

(1) Badi, N.; Lutz, J.-F. Sequence Control in Polymer Synthesis. *Chem. Soc. Rev.* **2009**, *38* (12), 3383−3390.

(2) Lutz, J.-F.; Ouchi, M.; Liu, D. R.; Sawamoto, M. Sequence-Controlled Polymers. *Science* **2013**, *341* (6146), 1238149

(3) Davidson, E. C.; Rosales, A. M.; Patterson, A. L.; Russ, B.; Yu, B.; Zuckermann, R. N.; Segalman, R. A. Impact of Helical Chain Shape in Sequence-Defined Polymers on Polypeptoid Block Copolymer Self-Assembly. *Macromolecules* **2018**, *51* (5), 2089−2098.

(4) Epps, T. H., III; O'Reilly, R. K. Block Copolymers: Controlling Nanostructure to Generate Functional Materials − Synthesis, Characterization, and Engineering. *Chem. Sci.* **2016**, *7* (3), 1674−1689.

(5) Le, D. N.; Hansen, E.; Khan, H. A.; Kim, B.; Wiest, O.; Dong, V. M. Hydrogenation Catalyst Generates Cyclic Peptide Stereocentres in Sequence. *Nat. Chem.* **2018**, *10*, 968.

(6) Low, J. Z.; Capozzi, B.; Cui, J.; Wei, S.; Venkataraman, L.; Campos, L. M. Tuning the Polarity of Charge Carriers Using Electron Deficient Thiophenes. *Chem. Sci.* **2017**, *8* (4), 3254−3259.

(7) Hirao, T.; Kudo, H.; Amimoto, T.; Haino, T. Sequence-Controlled Supramolecular Terpolymerization Directed by Specific Molecular Recognitions. *Nat. Commun.* **2017**, *8* (1), 634.

(8) Lutz, J.-F. Coding Macromolecules: Inputting Information in Polymers Using Monomer-Based Alphabets. *Macromolecules* **2015**, *48* (14), 4759−4767.

(9) Lytle, T. K.; Chang, L.-W.; Markiewicz, N.; Perry, S. L.; Sing, C. E. Designing Electrostatic Interactions via Polyelectrolyte Monomer Sequence. *ACS Cent. Sci.* **2019**, *5* (4), 709−718.

(10) Lutz, J.-F. Defining the Field of Sequence-Controlled Polymers. *Macromol. Rapid Commun.* **2017**, *38* (24), 1700582.

(11) Lutz, J.-F.; Ouchi, M.; Sawamoto, M.; Meyer, T. Y. Sequence-Controlled Polymers: Synthesis, Self-Assembly, and Properties. *ACS Symposium Series*; American Chemical Society, January 1, **2014**.

(12) Lutz, J.-F. Sequence-Controlled Polymerizations: The next Holy Grail in Polymer Science? *Polym. Chem.* **2010**, *1* (1), 55−62.

(13) Barnes, J. C.; Ehrlich, D. J. C.; Gao, A. X.; Leibfarth, F. A.; Jiang, Y.; Zhou, E.; Jamison, T. F.; Johnson, J. A. Iterative Exponential Growth of Stereo- and Sequence-Controlled Polymers. *Nat. Chem.* **2015**, *7*, 810.

(14) Yang, C.; Flynn, J. P.; Niu, J. Facile Synthesis of Sequence-Regulated Synthetic Polymers Using Orthogonal SuFEx and CuAAC Click Reactions. *Angew. Chem., Int. Ed.* **2018**, *57* (49), 16194−16199.

(15) Niu, J.; Hili, R.; Liu, D. R. Enzyme-Free Translation of DNA into Sequence-Defined Synthetic Polymers Structurally Unrelated to Nucleic Acids. *Nat. Chem.* **2013**, *5*, 282.

(16) Pfeifer, S.; Lutz, J.-F. A Facile Procedure for Controlling Monomer Sequence Distribution in Radical Chain Polymerizations. *J. Am. Chem. Soc.* **2007**, *129* (31), 9542−9543.

(17) Nowalk, J. A.; Fang, C.; Short, A. L.; Weiss, R. M.; Swisher, J. H.; Liu, P.; Meyer, T. Y. Sequence-Controlled Polymers Through Entropy-Driven Ring-Opening Metathesis Polymerization: Theory, Molecular Weight Control, and Monomer Design. *J. Am. Chem. Soc.* **2019**, *141* (14), 5741−5752.

(18) Kobayashi, S.; Pitet, L. M.; Hillmyer, M. A. Regio- and Stereoselective Ring-Opening Metathesis Polymerization of 3-Substituted Cyclooctenes. *J. Am. Chem. Soc.* **2011**, *133* (15), 5794−5797.

(19) Satoh, K.; Ozawa, S.; Mizutani, M.; Nagai, K.; Kamigaito, M. Sequence-Regulated Vinyl Copolymers by Metal-Catalysed Step-Growth Radical Polymerization. *Nat. Commun.* **2010**, *1*, 6.

(20) Li, T.; Liu, L.; Wei, N.; Yang, J.-Y.; Chapla, D. G.; Moremen, K. W.; Boons, G.-J. An Automated Platform for the Enzyme-Mediated Assembly of Complex Oligosaccharides. *Nat. Chem.* **2019**, *11* (3), 229−236.

(21) Li, J.; Ballmer, S. G.; Gillis, E. P.; Fujii, S.; Schmidt, M. J.; Palazzolo, A. M. E.; Lehmann, J. W.; Morehouse, G. F.; Burke, M. D. Synthesis of Many Different Types of Organic Small Molecules Using One Automated Process. *Science (Washington, DC, U. S.)* **2015**, *347* (6227), 1221−1226.

(22) Lewandowski, B.; De Bo, G.; Ward, J. W.; Papmeyer, M.; Kuschel, S.; Aldegunde, M. J.; Gramlich, P. M. E.; Heckmann, D.; Goldup, S. M.; D'Souza, D. M.; et al. Sequence-Specific Peptide Synthesis by an Artificial Small-Molecule Machine. *Science (Washington, DC, U. S.)* **2013**, *339* (6116), 189−193.

(23) Lawrence, J.; Goto, E.; Ren, J. M.; McDearmon, B.; Kim, D. S.; Ochiai, Y.; Clark, P. G.; Laitar, D.; Higashihara, T.; Hawker, C. J. A Versatile and Efficient Strategy to Discrete Conjugated Oligomers. *J. Am. Chem. Soc.* **2017**, *139* (39), 13735−13739.

(24) Liang, L.; Wang, J.-T.; Xiang, X.; Ling, J.; Zhao, F.-G.; Li, W.-S. Influence of Moiety Sequence on the Performance of Small Molecular Photovoltaic Materials. *J. Mater. Chem. A* **2014**, *2* (37), 15396−15405.

(25) Roy, R. K.; Lutz, J.-F. Compartmentalization of Single Polymer Chains by Stepwise Intramolecular Cross-Linking of Sequence-Controlled Macromolecules. *J. Am. Chem. Soc.* **2014**, *136* (37), 12888−12891.

(26) Palermo, E. F.; McNeil, A. J. Impact of Copolymer Sequence on Solid-State Properties for Random, Gradient and Block

Copolymers Containing Thiophene and Selenophene. *Macromolecules* **2012**, *45* (15), 5948−5955.
(27) Zhang, S.; Bauer, N. E.; Kanal, I. Y.; You, W.; Hutchison, G. R.; Meyer, T. Y. Sequence Effects in Donor−Acceptor Oligomeric Semiconductors Comprising Benzothiadiazole and Phenylenevinylene Monomers. *Macromolecules* **2017**, *50* (1), 151−161.
(28) Fortney, A.; Tsai, C.-H.; Banerjee, M.; Yaron, D.; Kowalewski, T.; Noonan, K. J. T. Impact of Precise Control over Microstructure in Thiophene−Selenophene Copolymers. *Macromolecules* **2018**, *51* (23), 9494−9501.
(29) Patterson, A. L.; Danielsen, S. P. O.; Yu, B.; Davidson, E. C.; Fredrickson, G. H.; Segalman, R. A. Sequence Effects on Block Copolymer Self-Assembly through Tuning Chain Conformation and Segregation Strength Utilizing Sequence-Defined Polypeptoids. *Macromolecules* **2019**, *52* (3), 1277−1286.
(30) Sun, J.; Liao, X.; Minor, A. M.; Balsara, N. P.; Zuckermann, R. N. Morphology-Conductivity Relationship in Crystalline and Amorphous Sequence-Defined Peptoid Block Copolymer Electrolytes. *J. Am. Chem. Soc.* **2014**, *136* (42), 14990−14997.
(31) Xin, N.; Guan, J.; Zhou, C.; Chen, X.; Gu, C.; Li, Y.; Ratner, M. A.; Nitzan, A.; Stoddart, J. F.; Guo, X. Concepts in the Design and Engineering of Single-Molecule Electronic Devices. *Nat. Rev. Phys.* **2019**, *1* (3), 211−230.
(32) Meier, M. A. R.; Barner-Kowollik, C. A New Class of Materials: Sequence-Defined Macromolecules and Their Emerging Applications. *Adv. Mater.* **2019**, *31* (26), 1806027.
(33) Capozzi, B.; Dell, E. J.; Berkelbach, T. C.; Reichman, D. R.; Venkataraman, L.; Campos, L. M. Length-Dependent Conductance of Oligothiophenes. *J. Am. Chem. Soc.* **2014**, *136* (29), 10486−10492.
(34) Yin, X.; Zang, Y.; Zhu, L.; Low, J. Z.; Liu, Z.-F.; Cui, J.; Neaton, J. B.; Venkataraman, L.; Campos, L. M. A Reversible Single-Molecule Switch Based on Activated Antiaromaticity. *Sci. Adv.* **2017**, *3* (10), eaao2615.
(35) Moreno-Garcia, P.; Gulcur, M.; Manrique, D. Z.; Pope, T.; Hong, W.; Kaliginedi, V.; Huang, C.; Batsanov, A. S.; Bryce, M. R.; Lambert, C.; et al. Single-Molecule Conductance of Functionalized Oligoynes: Length Dependence and Junction Evolution. *J. Am. Chem. Soc.* **2013**, *135* (33), 12228−12240.
(36) Zhang, N.; Lo, W.-Y.; Cai, Z.; Li, L.; Yu, L. Molecular Rectification Tuned by Through-Space Gating Effect. *Nano Lett.* **2017**, *17* (1), 308−312.
(37) Bai, J.; Daaoub, A.; Sangtarash, S.; Li, X.; Tang, Y.; Zou, Q.; Sadeghi, H.; Liu, S.; Huang, X.; Tan, Z.; Liu, J.; Yang, Y.; Shi, J.; Mészáros, G.; Chen, W.; Lambert, C.; Hong, W. Anti-Resonance Features of Destructive Quantum Interference in Single-Molecule Thiophene Junctions Achieved by Electrochemical Gating. *Nat. Mater.* **2019**, *18* (4), 364−369.
(38) Aragonès, A. C.; Darwish, N.; Im, J.; Lim, B.; Choi, J.; Koo, S.; Díez-Pérez, I. Fine-Tuning of Single-Molecule Conductance by Tweaking Both Electronic Structure and Conformation of Side Substituents. *Chem. - Eur. J.* **2015**, *21* (21), 7716−7720.
(39) Chen, F.; Tao, N. J. Electron Transport in Single Molecules: From Benzene to Graphene. *Acc. Chem. Res.* **2009**, *42* (3), 429−438.
(40) van Leusen, A. M.; Siderius, H.; Hoogenboom, B. E.; van Leusen, D. A New and Simple Synthesis of the Pyrrole Ring System from Michael Acceptors and Tosylmethylisocyanides. *Tetrahedron Lett.* **1972**, *13* (52), 5337−5340.
(41) Li, B.; Yu, H.; Montoto, E. C.; Liu, Y.; Li, S.; Schwieter, K.; Rodríguez-López, J.; Moore, J. S.; Schroeder, C. M. Intrachain Charge Transport through Conjugated Donor−Acceptor Oligomers. *ACS Appl. Electron. Mater.* **2019**, *1* (1), 7−12.
(42) Aradhya, S. V.; Venkataraman, L. Single-Molecule Junctions beyond Electronic Transport. *Nat. Nanotechnol.* **2013**, *8*, 399.
(43) Su, T. A.; Neupane, M.; Steigerwald, M. L.; Venkataraman, L.; Nuckolls, C. Chemical Principles of Single-Molecule Electronics. *Nat. Rev. Mater.* **2016**, *1* (3), 16002.
(44) Venkataraman, L.; Klare, J. E.; Nuckolls, C.; Hybertsen, M. S.; Steigerwald, M. L. Dependence of Single-Molecule Junction Conductance on Molecular Conformation. *Nature* **2006**, *442* (7105), 904−907.
(45) Zotti, L. A.; Kirchner, T.; Cuevas, J.-C.; Pauly, F.; Huhn, T.; Scheer, E.; Erbe, A. Revealing the Role of Anchoring Groups in the Electrical Conduction Through Single-Molecule Junctions. *Small* **2010**, *6* (14), 1529−1535.
(46) Kaliginedi, V.; Rudnev, A. V.; Moreno-Garcia, P.; Baghernejad, M.; Huang, C.; Hong, W.; Wandlowski, T. Promising Anchoring Groups for Single-Molecule Conductance Measurements. *Phys. Chem. Chem. Phys.* **2014**, *16* (43), 23529−23539.
(47) Li, S.; Yu, H.; Schwieter, K.; Chen, K.; Li, B.; Liu, Y.; Moore, J. S.; Schroeder, C. M. Charge Transport and Quantum Interference Effects in Oxazole-Terminated Conjugated Oligomers. *J. Am. Chem. Soc.* **2019**, *141* (40), 16079−16084.
(48) Leary, E.; La Rosa, A.; González, M. T.; Rubio-Bollinger, G.; Agraït, N.; Martín, N. Incorporating Single Molecules into Electrical Circuits. The Role of the Chemical Anchoring Group. *Chem. Soc. Rev.* **2015**, *44* (4), 920−942.
(49) Miguel, D.; Alvarez de Cienfuegos, L.; Martin-Lasanta, A.; Morcillo, S. P.; Zotti, L. A.; Leary, E.; Burkle, M.; Asai, Y.; Jurado, R.; Cardenas, D. J.; et al. Toward Multiple Conductance Pathways with Heterocycle-Based Oligo(Phenyleneethynylene) Derivatives. *J. Am. Chem. Soc.* **2015**, *137* (43), 13818−13826.
(50) Kamenetska, M.; Koentopp, M.; Whalley, A. C.; Park, Y. S.; Steigerwald, M. L.; Nuckolls, C.; Hybertsen, M. S.; Venkataraman, L. Formation and Evolution of Single-Molecule Junctions. *Phys. Rev. Lett.* **2009**, *102* (12), 126803.
(51) Kim, N. T.; Li, H.; Venkataraman, L.; Leighton, J. L. High-Conductance Pathways in Ring-Strained Disilanes by Way of Direct σ-Si−Si to Au Coordination. *J. Am. Chem. Soc.* **2016**, *138* (36), 11505−11508.
(52) Cai, Z.; Zhang, N.; Awais, M. A.; Filatov, A. S.; Yu, L. Synthesis of Alternating Donor−Acceptor Ladder-Type Molecules and Investigation of Their Multiple Charge-Transfer Pathways. *Angew. Chem., Int. Ed.* **2018**, *57* (22), 6442−6448.
(53) Su, T. A.; Li, H.; Steigerwald, M. L.; Venkataraman, L.; Nuckolls, C. Stereoelectronic Switching in Single-Molecule Junctions. *Nat. Chem.* **2015**, *7*, 215.
(54) Su, T. A.; Li, H.; Zhang, V.; Neupane, M.; Batra, A.; Klausen, R. S.; Kumar, B.; Steigerwald, M. L.; Venkataraman, L.; Nuckolls, C. Single-Molecule Conductance in Atomically Precise Germanium Wires. *J. Am. Chem. Soc.* **2015**, *137* (38), 12400−12405.
(55) Catalán, J.; Elguero, J. Basicity of Azoles. IV. Empirical Relationships between Basicity and Ionization Potential for Aromatic Five Membered Rings Containing Nitrogen or Oxygen. *J. Heterocycl. Chem.* **1984**, *21* (1), 269−270.

https://dx.doi.org/10.1021/jacs.0c00043
J. Am. Chem. Soc. 2020, 142, 4852−4861